Influence of flow-interruption on filter performance during the filtration of liquid aerosols by fibrous filters

Arne Bredin[1] *, Benjamin J. Mullins[1,2]

[1] Fluid Dynamics Research Group, Curtin University,

[2] Curtin Health Innovation Research Institute,

GPO Box U1987, Perth WA 6845, Australia

*Corresponding author. Fax: +61 8 9266 4811

E-mail address: arne.bredin@postgrad.curtin.edu.au (A. Bredin)

Abstract:

This study investigated the influence of flow interruptions on the filtration performance of two different multi-layered fibrous filters during liquid aerosol filtration. It was found that both types of filters experienced a significant secondary loading stage, though they had reached a steady state for continuous flow. The filters showed distinctive increases in pressure drop and filter saturation until a second equilibrium state was reached. This second equilibrium state was attributed to a rearrangement of liquid in the filter during the breaks, clogging previously free passages. The ratio of shear and capillary forces was found to determine whether these passages were able to be “cleaned” once airflow was recommenced. Based on these findings, the airflow required to clean fully saturated filters was investigated and a phenomenological model developed to describe this behaviour. Furthermore, it was found that filters could be cleaned and reused, whereby they would return to one of the previous steady states (continuous or discontinuous flow). The experiments conducted in this work represent a more realistic test for oil-mist (or coalescing) filters than typical laboratory testing. Furthermore, it is hoped that they will help to bridge the gap between laboratory and field test results.

Keywords: flow interruption, aerosol, filtration, capillary, filter cleaning

Nomenclature

Acronyms

EQ1	at first equilibrium state
EQ2	at second equilibrium state
N	normalized

Greek letters

α	packing density
γ	surface tension
ΔP	filter pressure drop
v	kinematic viscosity
μ	dynamic viscosity
θ	meniscus contact angle
ρ_{Oil}	oil density

Latin letters

c_{in} , c_{out}	particle concentration before / after the filter
d_{cap}	capillary diameter
d_f	fibre diameter

d_{mean}	mean diameter of the capillary size distribution
E	filter efficiency
$l(t)$	distance of the gas-liquid interface from capillary tube inlet (time dependant)
m_{Filter}	mass of the filter and oil
$m_{Filter,0}$	initial mass of the clean filter
m_{Oil}	mass of oil held in the filter
$m_{Oil,max}$	maximum oil capacity (mass) of the filter
$\dot{m}_{Drain}$	oil mass (flow) draining from the filter
$\dot{m}_{Oil,in}$	oil loading mass (flow)
$\dot{m}_{Oil,out}$	oil mass (flow) after the filter
n_{Cycle}	filtration cycle number
$P_{l,0}$, $P_{l,m}$	liquid pressure at the start of the capillary / at the gas-liquid interface
P_g	gas pressure
S	filter saturation
S_R	filter saturation after filter regeneration
S_{calc}	calculated filter saturation
S_{exp}	experimental filter saturation
t	time
V_{Oil}	volume of oil in the filter

1 Introduction

Filtration is used in many industries to remove aerosols from process streams in order to maintain hygienic, environmental or production standards. Although the filtration of solid particles using fibrous filter media has received significant research and is widely explored, the mechanisms of mist filtration and filter clogging with droplets are yet not fully understood and mist filter development is largely conducted empirically at present. An increasing number of publications can, however, be found describing loading and clogging mechanisms of mist filters.

For oleophillic filters, it has been suggested [1] that the filter loading process can be divided into four distinct steps. During the first step, the filter is wetted by deposited liquid particles and a thin film around the fibres is formed. This film interferes only minimally with the airflow, however reduces the fibre collection area [2] and therefore the pressure drop increases very slowly during this phase whereas the filter penetration increases rapidly (particularly for submicron droplets). The second step is characterized by the formation of droplets on the fibres since the film will be broken up due to Plateau-Rayleigh instability [3], [4]. The droplets can coalesce and form bigger drops on the fibre surface [5] and bridges between fibres, leading to an exponential increase in penetration which is again attributed to the decrease in fibre collection area. The pressure drop starts to increase more rapidly during this phase. In the third step, the interstices between fibres close more and more [6], leading to a massive increase in the pressure drop. It has been reported [6], [1] that penetration of larger particles decreases in this phase due to increased inertial deposition caused by high interstitial flow velocities. However, this is not the case for all filters [5], [7]. Once a certain threshold of oil in the filter is attained, the filter now reaches a stationary state (“equilibrium state”). In this

stage pressure drop and filter penetration are constant and liquid drains from the filter at the same rate at which it is captured.

Almost all previous studies of mist filtration [1], [6], [8], [9] have been conducted using constant aerosol flow and loading rates. However, typical filtration systems such as used in air compressors or automotive applications are mainly operated discontinuously (cessation of flow for extended periods of time in which both air flow and aerosol generation are discontinued), or with significant variations in flow rate. To the knowledge of the authors this issue has rarely been examined in published literature, with the exception of Frising et al. [10] who demonstrated that after a break in aerosol flow, the pressure drop of a HEPA filter collecting oil aerosol increased when the aerosol flow was engaged again. This phenomenon however was only examined with one start-stop cycle. Indeed, in most cases, aerosol generation was stopped however clean air was still flowing through the filter, which is quite different to the scenario in "real world" applications.

This work investigates the filtration behaviour of aerosol filters during long-term discontinuous operation, as occurs in “real world” applications. Industrial oil mist filters were tested in continuous and discontinuous operation. The filters were first preloaded until they reached an equilibrium state, then operated discontinuously (the aerosol flow stopped at regular intervals). The behaviour of the filters during discontinuous operation was investigated and the influence of different filtration and break interval durations was evaluated. The air flow rate necessary to remove accumulated oil from the filters was also investigated, using a method similar to the “pulse-jet“ cleaning of surface (dust) filters.

A phenomenological model was developed to show the relationship between pressure drop and the saturation during the initial cleaning of a fully saturated filter. This model was also able to show the effect of different “effective” capillary diameters in a filter on the cleaning behaviour.

2 Experimental Apparatus and Methods

2.1 Filter Testing Apparatus

The filtration experiments were conducted using a specially developed testing apparatus as shown in Fig. 1. The test aerosol was generated using a 3-jet Collison nebulizer. After dilution with clean HEPA filtered air, the aerosol was passed through the test filter chamber using a DVP SB10 vacuum pump (D.V.P. Vacuum Technology, Italy) at a flow rate of 55 LPM controlled by a critical orifice. The test filters were two types of commercially manufactured automotive crankcase filters (MANN+HUMMEL GmbH, Germany).

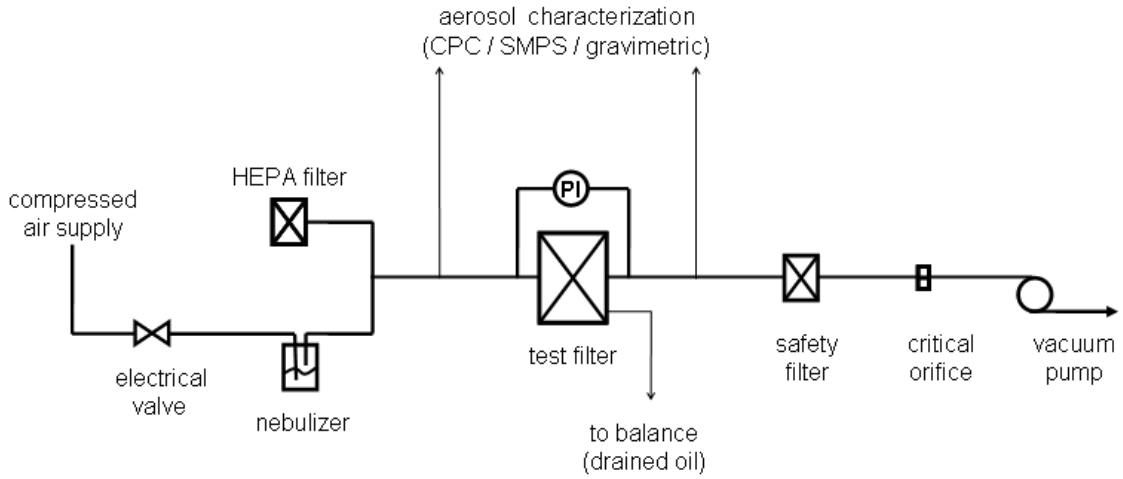

Fig. 1: Experimental apparatus for filter testing. The solenoid valve on the compressed air supply allowed the nebulizer to be switched on and off.

The pressure drop of the filter was measured using a differential pressure sensor (SenSym SDX01D4, SensorTechnics, Germany). Iso-kinetic sample points before and after the filter allowed filtration efficiency monitoring using a Condensation Particle Counter (CPC) (TSI 3775, TSI Inc., WN, USA) or a Scanning Mobility Particle Sizer, consisting of the same CPC and a Differential Mobility Analyzer (DMA) (TSI 3010, TSI Inc., WN, USA). These sample points were also used for gravimetric measurements. The oil draining from the bottom of the filter chamber was collected in a vessel mounted on an analytical balance (GX400, A&D Engineering Inc., CA, USA). The entire balance was housed in a pressurised vessel at the same pressure as the filter chamber and the drainage hose from the filter chamber was not in contact with the collection can.

The compressed air supply valve for the nebulizer and the vacuum pump were controlled by a timer which allowed airflow and aerosol generation to be stopped simultaneously during discontinuous operation.

2.2 Engine Oil

Castrol RX Super (Castrol Ltd., UK) oil was used in this work as the test aerosol as it is a common diesel engine lubricant for subtropical conditions. The relevant properties of RX Super are ρ_{Oil} = 0.873 kg/L and v = 114 cSt at 40 °C.

The particle size distribution of the oil aerosol used to challenge the filter can be seen in Fig. 2 (as measured by SMPS). The volume-mean diameter was calculated as 510 ±1.5 nm from SMPS measurements, however 850 ±17 nm from gravimetric measurements divided by CPC counts, which is likely more accurate, as the large particles which cannot be counted by SMPS would possess nontrivial mass. Gravimetric measurements showed a mass loading rate of approximately 182 ±3.3 mg/m^3 which was in close agreement to measurements (175 ±4.3 mg/m^3) using a DUSTTRAK aerosol monitor (TSI, TSI Inc., WN, USA).

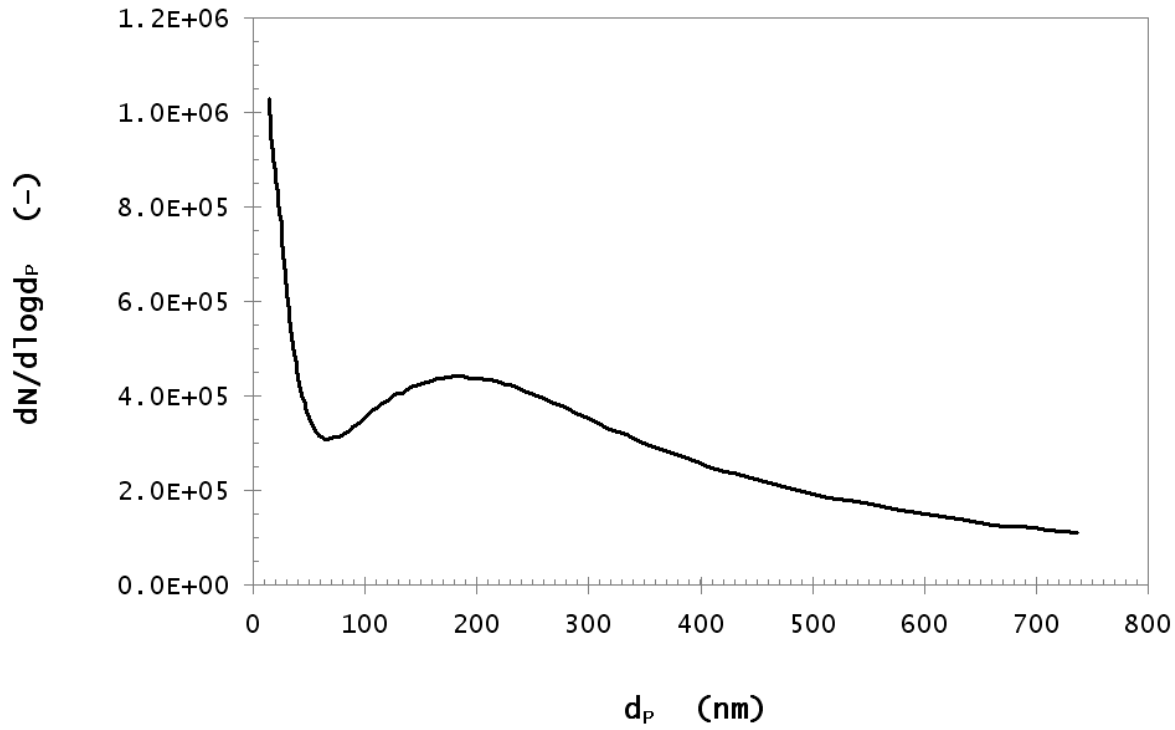

Fig. 2: Particle size distribution of the aerosol used to challenge the filters (measured by SMPS).

2.3 Filter characterisation

Two different commercially available filters (MANN + HUMMEL GmbH, Germany) were used in this work. The filters were of cylindrical construction with the air flowing from the inside to the outside of the element. The filter element consisted of an inner support mesh, which was wrapped with layers of nonwoven stainless steel fibrous media. Each layer consisted of fibres of only one (mean) diameter d_f. The two different filter elements used in this work were designated Filter A and Filter B, their properties are shown in Table 1.

Table 1: Properties of the oil mist filters (filter media only) used in this work.

	Filter A	**Filter B**
Fibre material	Stainless Steel 316	Stainless Steel 316
Number of layers	4	3
d_f (µm)	4.2	2.3, 7.8
α (-)	0.024	0.019
$m_{Oil,max}$ (g)	56.61 ±0.7	50.01 ±0.4
Total mass of filter media (g)	12.1 ±0.15	13.3 ±0.2
Filter face velocity (cm/s)	6.8	6.8
Height (mm)	91 ±0.5	91 ±1.1
Outside diameter (mm)	56 ±1.4	55 ±1.3
Thickness (mm)	9.±0.6	8 ±0.7

All values determined by the authors.

2.4 Filter preloading and continuous filtration operation

The experimental procedure was divided into three steps, as follows

- The preloading stage: the filter was preloaded to accelerate the attainment of the equilibrium state. This stage was omitted for filters without preloading
- Saturation stage: the filter was continuously exposed to the standard aerosol concentration until saturated (first equilibrium state EQ_1)
- Cycling stage: the filter underwent discontinuous operation with “stop-and-go” cycles

Two different filter preloading methods were used in this work:

Method I: Dipping And Draining (*DAD*): The filter was preloaded by submerging it into oil (the same oil as used in the experiment) for 18 hours and then withdrawn and held upright for 6 hours to allow excessive oil to drain.

Method II: Rapid Aerosol Saturation (*RAS*): The filter was exposed to a higher aerosol concentration (two times higher than that used in the experiments) for approximately 40 hours.

Both preloading methods were proven not to influence the steady state filter saturation and subsequent experiments – see section 3.1. After the preloading process, filters were inserted into the filter chamber, where they were exposed to the stated aerosol concentration. Filters that were not preloaded using either accelerated method were exposed to this concentration from the start. The filter was considered to have reached the first equilibrium state EQ_1 when pressure drop and the drainage did not change significantly.

2.5 Discontinuous filter operation

After the filter attained the first equilibrium state EQ_1, it was subjected to discontinuous cyclic operation. A timer controlled electric switch simultaneously engaged and disengaged both the aerosol generation and the air flow through the filter chamber. The combination of a flow and a break represents one “cycle”. This procedure was then repeated until a new equilibrium state EQ_2 was reached.

2.6 Filter Regeneration

Filters were “regenerated” by removing oil from the filter using a higher than normal flow rate of air through the filter. Regeneration was conducted “off-line” using a specially constructed apparatus which injected compressed air into the top of the filter (in flow direction unlike common “reverse-pulse” cleaning of dust filters). Airflow was continued until no further oil was observed to drain. The drained oil was collected and its mass was measured on a balance after the cleaning process was complete.

2.7 Mass and Efficiency Measurements

The filter (and oil) mass was determined by carefully removing the filter from the filter chamber and weighing it during breaks in airflow. Preliminary experiments proved that this process did not affect the pressure drop, mass or drainage behaviour of the filter. A balance (GX400 analytical balance, A&D Engineering Inc., CA, USA) was used for all mass measurements.

The (number based) filtration efficiency E was determined by alternately monitoring the upstream (c_{in}) and downstream (c_{out}) particle concentration in the aerosol stream by CPC or SMPS and can be calculated as

$$E = 1 - \frac{c_{out}}{c_{in}} \tag{1}$$

For fractional efficiency, c_{in} and c_{out} represent the vales for one particle aerosol size class.

Gravimetric filtration efficiency was measured using a sampling probe with a diameter of 2.5 mm at a sample flow of 1.5 LPM to ensure iso-kinetic sampling. The sample was collected on a HEPA filter (Nalgene, Thermo Fisher Scientific, MA, USA) using a sampling period of 60 min.

The maximum oil capacity $m_{Oil,max}$ of the filter media can be defined as the theoretical amount of oil $m_{Oil,max}$ which the filter media can contain when fully saturated, i.e. all available void space is filled with oil. This value was obtained by calculation and experimental measurement and it was found that both methods showed a good agreement (less than 1.5% difference for each filter type). The filter saturation S is the ratio between the oil mass held in the filter and $m_{Oil,max}$, and can be calculated as

$$S = \frac{m_{Oil}}{m_{\mathrm{Oil,max}}} = \frac{V_{Oil}\rho_{Oil}}{m_{Oil,\mathrm{max}}} = \frac{m_{Filter} - m_{Filter,0}}{m_{Oil,\mathrm{max}}} \tag{2}$$

with m_{Oil} being the mass of the oil held in the filter, m_{Filter} the mass of the filter and oil together, $m_{Filter,0}$ the initial mass of the clean filter. The saturation at the equilibrium states is assigned as S_{EQ1} or S_{EQ2} and the saturation after filter regeneration as S_R.

To estimate the amount of oil in the filter during the “on”-steps, a mass balance was conducted, as follows

$$\frac{dm_{Oil}}{dt} = \dot{m}_{Oil,in} - \dot{m}_{Oil,out} - \dot{m}_{Drain} \tag{3}$$

with $\dot{m}_{Oil,in}$ being the oil loading mass flow, $\dot{m}_{Drain}$ the mass flow of drained oil and $\dot{m}_{Oil,out}$ the mass flow of oil passing the filter (not captured). It was assumed that the flow rate into and out of the filter was constant during the majority of the on-step. A time-lag for oil to transit the drainage hose from the filter was observed to be approximately 2.5 seconds. This was assumed negligible in comparison to other experimental timescales, so results were not corrected for this.

3 Results and discussion

3.1 Validation of filter loading methods

Although dipping filters to accelerate the loading process is commonly used in industry, there exists no literature on this topic. Therefore, preliminary experiments were conducted to ensure that both preloading methods lead to the same equilibrium state (EQ_1) for continuous operation. Fig. 3 shows a comparison of the 3 different (pre)loading methods (*DAD*, *RAS* and no preloading). It was found that filters preloaded using the *DAD* or the *RAS* method exhibited the same filtration behaviour as a filters saturated entirely with aerosol at the normal rate.

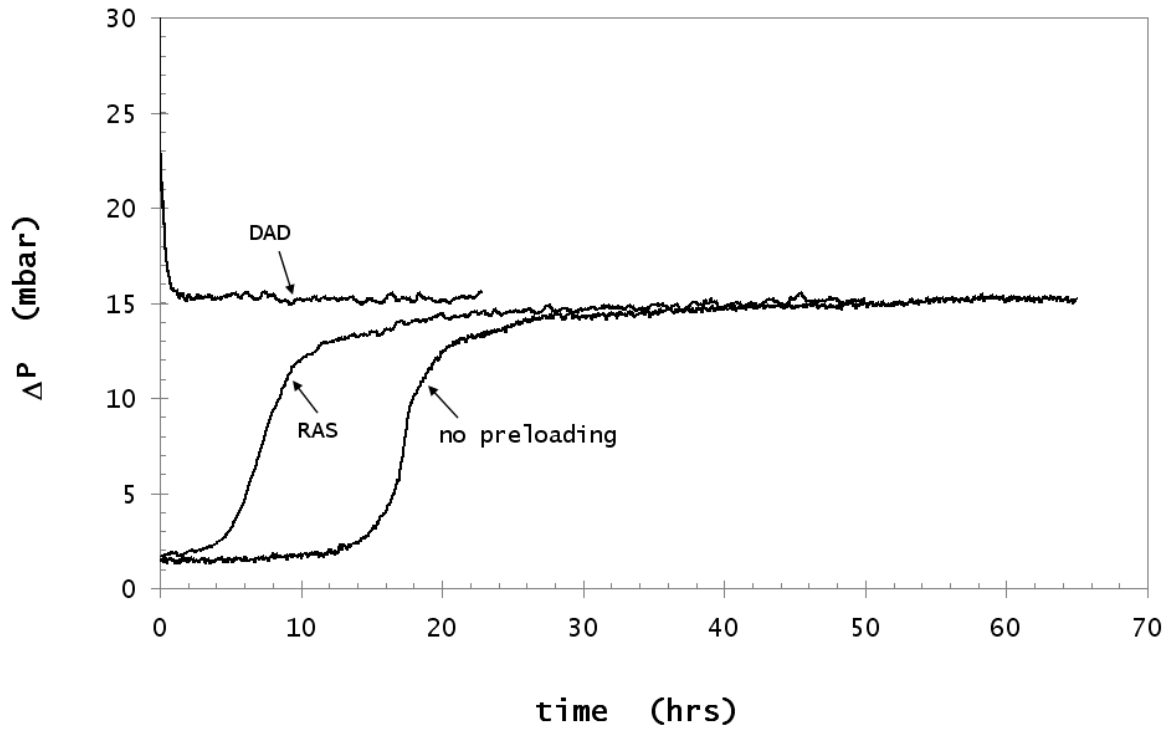

Fig. 3: Validation of the RAS and DAD preloading method against an experiment without preloading (Filter type A). The pressure drop axis is set at 30 mbar maximum, however the initial reading DAD filters were >70 mbar. No significant difference in ΔP_{EQ1} was observed between the different loading methods.

It can clearly be seen in Fig. 3 that after a sufficient period of time both preloaded filters attained a similar pressure drop ΔP_{EQ1} as the non preloaded filter: ΔP_{EQ1} = 15.2 mbar for the *RAS* method, 15.4 mbar for the *DAD* and 15.2 mbar for the filter without preloading. Drainage rates and filter saturation were nearly identical for all preloading methods with $\dot{m}_{Drain,EQ1}$ = 142 ±5.2 mg/m^3 and S_{EQ1} = 0.61 ±0.04.

Filters preloaded using the *DAD* method were considered to initially be fully saturated (S = 1) with all void space between fibres filled with liquid. Hence, there were no free passages in

the filter through which the air could flow, resulting in an extremely high pressure drop of the filter immediately after air flow is applied (in this case >70 mbar). The extremely elevated pressure drop and high shear forces occurring during the first seconds of filtration expel the oil out of the filter, creating initial passages through the filter. The high interstitial velocities (and thus high shear forces) are due to all airflow being forced through a small number of narrow free passages in the filter. As oil is expelled from the filter, the number of passages increases and local interstitial velocities decrease – which continues until the filter reaches an equilibrium state.

3.2 The second equilibrium state (EQ_2) during discontinuous operation

Once equilibrium saturation (S_{EQ1}) and pressure drop (ΔP_{EQ1}) were reached, the filters were subjected to discontinuous operation. Air and aerosol flow were stopped for 120 minute intervals and recommenced for 120 minute intervals (120/120). To simplify the presentation of results from experiments with several dozen cycles the “on” pressure drop values of each cycle were averaged and divided by the average pressure drop ΔP_{EQ1} at the first equilibrium state, thus giving the normalized pressure drop ΔP_N for each cycle. The determination of the normalized drainage mass $m_{Drain,N}$ was calculated using the same method.

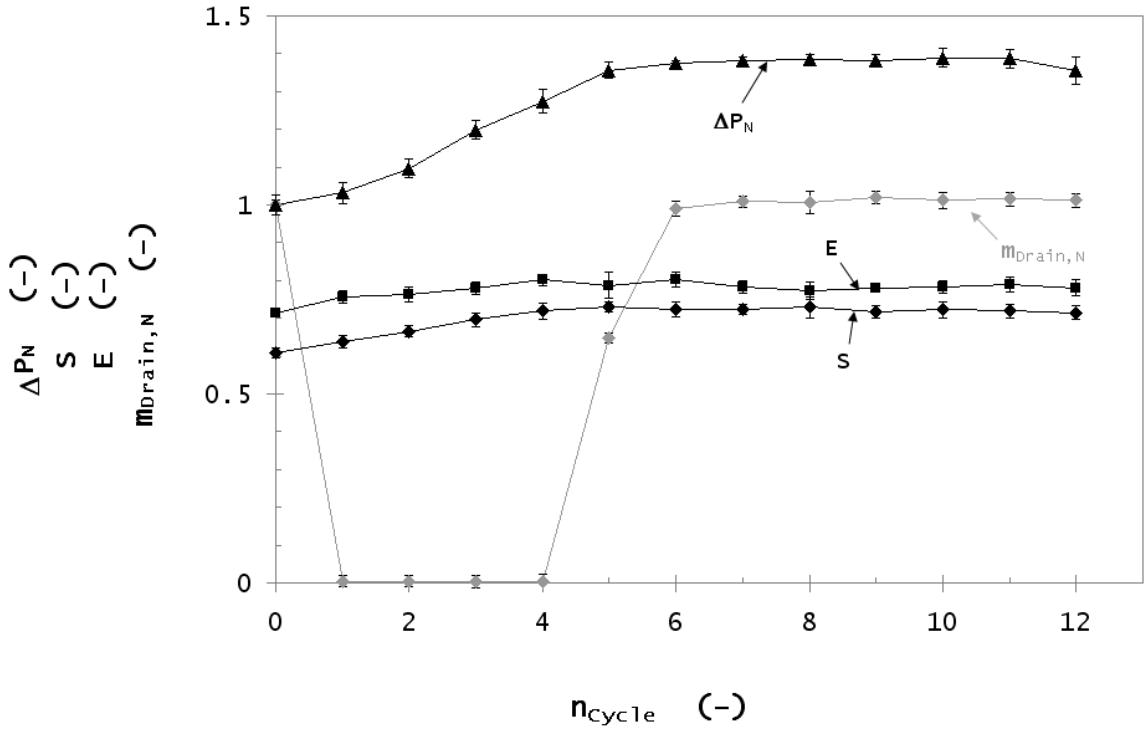

Fig. 4: Normalized pressure drop ΔP_N, normalized drainage rate $m_{Drain,N}$, filter efficiency E and saturation S per cycle of the Type A filters, during discontinuous operation. n_{Cycle} #0 represents the filter conditions during the first equilibrium state EQ_1 before the flow was initially discontinued.

The evolution of the normalized pressure drop ΔP_N and drainage rate for all cycles of the experiment is shown in Fig. 4. The curves are averaged from four experiments and the variation is represented by error bars. It can be seen that the reproducibility of the curves was excellent. The pressure drop increased during the first 5 cycles beyond ΔP_{EQ1} reaching a second stationary level ΔP_{EQ2} in cycle #6 as can be seen in Fig. 4. This new level was approximately 38% greater than the pressure drop during the first equilibrium state and once reached was found to be stable (i.e. the filter would not go back to ΔP_{EQ1}). During this period the drainage rate decreased from its equilibrium value to nearly zero and - after the second equilibrium state (EQ_2) was reached - returned to a similar rate as before.

According to (3) it is evident that – assuming a constant mass loading rate and capture efficiency - a change in drainage rate must produce a change in filter saturation. Since the aerosol mass entering and exiting the filter remained constant, this assumption was considered correct. The filter saturation S is displayed in Fig. 4. Once discontinuous operation commenced, the saturation increased simultaneously with an increase in pressure drop and a cessation of drainage. These findings suggest that the filter underwent a second loading stage after discontinuous operation commenced and was capable of storing further oil inside until reaching a second equilibrium state with a saturation S_{EQ2} of 0.72 in comparison to a saturation S_{EQ1} of 0.61 during the first equilibrium state.

The gravimetric overall collection efficiency E is also shown in Fig. 4 with Fig. 5 showing the fractional efficiencies. E was found to increase from an average of approximately 70% at EQ_1 to approximately 78% at EQ_2. The slight increase in efficiency was found only in the larger (interception and inertia dominated) size ranges, so is therefore likely due to the higher saturation of the filter as was found by some authors [5]. However, since the efficiency of the new filter is higher, this is counter-intuitive. A more likely explanation is that the re-arrangement of the oil has made the air flow paths through the filter more tortuous, thereby increasing particle capture.

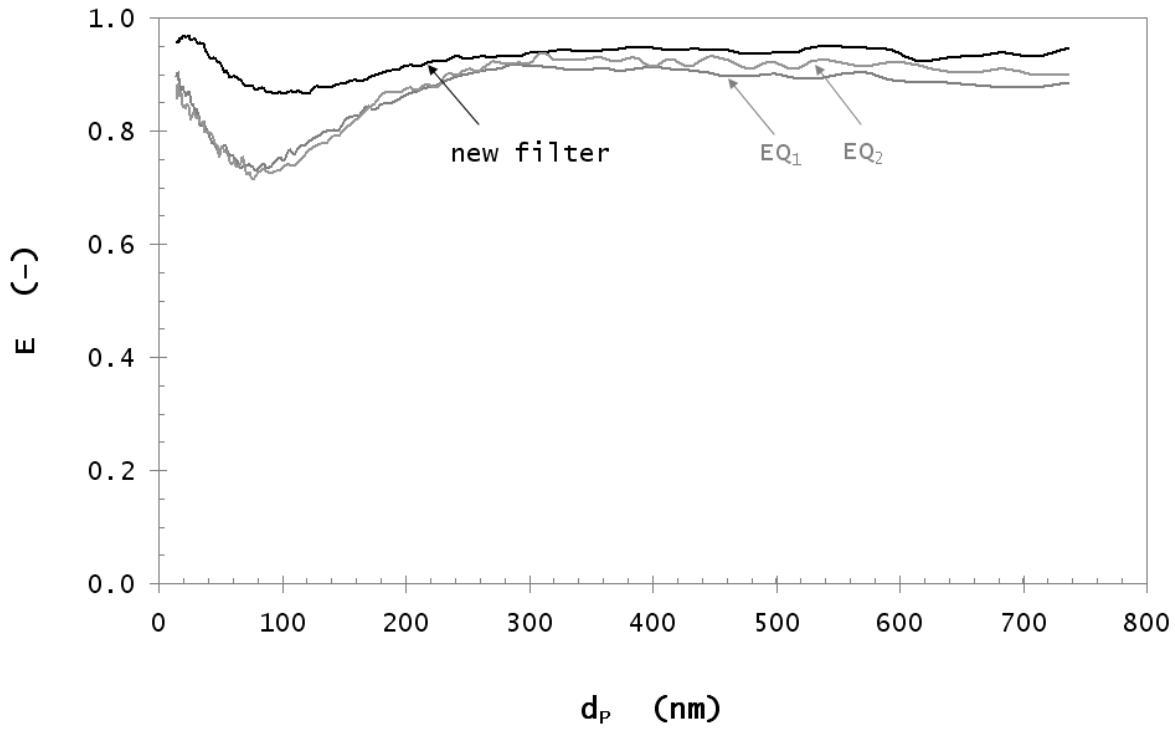

Fig. 5: Number-based filtration efficiency of a new filter and at the first and second equilibrium state EQ_1 and EQ_2.

The secondary loading phase and second steady state found is believed to be due to the rearrangement of oil in the filter after air flow was discontinued. The lack of shear forces allows capillary and gravitational forces to move oil into locations where it previously was not present (i.e. airflow channels). Furthermore, oil that has already been expelled from the filter, yet remains on the surface can be drawn back into the filter through capillarity, where it can block passages, causing an additional flow resistance. If shear forces from the recommencing airflow are too weak to clean these passages, the oil will remain in the filter leading to a higher saturation and a higher pressure drop. If more oil is stored in the filter and hence more passages are blocked during each break, then higher local velocities will be induced through the remaining free passages in the filter. Thus shear forces will increase locally and are now able to overcome capillary forces and clean passages of smaller

diameters than before. The ability to locally clean the filter and therefore the ratio between capillary forces (i.e. the number of clogged passages) and shear forces (i.e. the number of cleaned passages) is believed to be the predominant reason for the observed filter behaviour. If both forces are equal after each break in airflow, then the second equilibrium state EQ_2 is reached.

The rearrangement of oil in the filter is believed not to be an instantaneous process, but rather requires some time for the relatively viscous oil droplets to flow (and due to the slow nature of capillary flow). Fig. 6 shows the result of an experiment conducted with two different stop-and-go intervals.

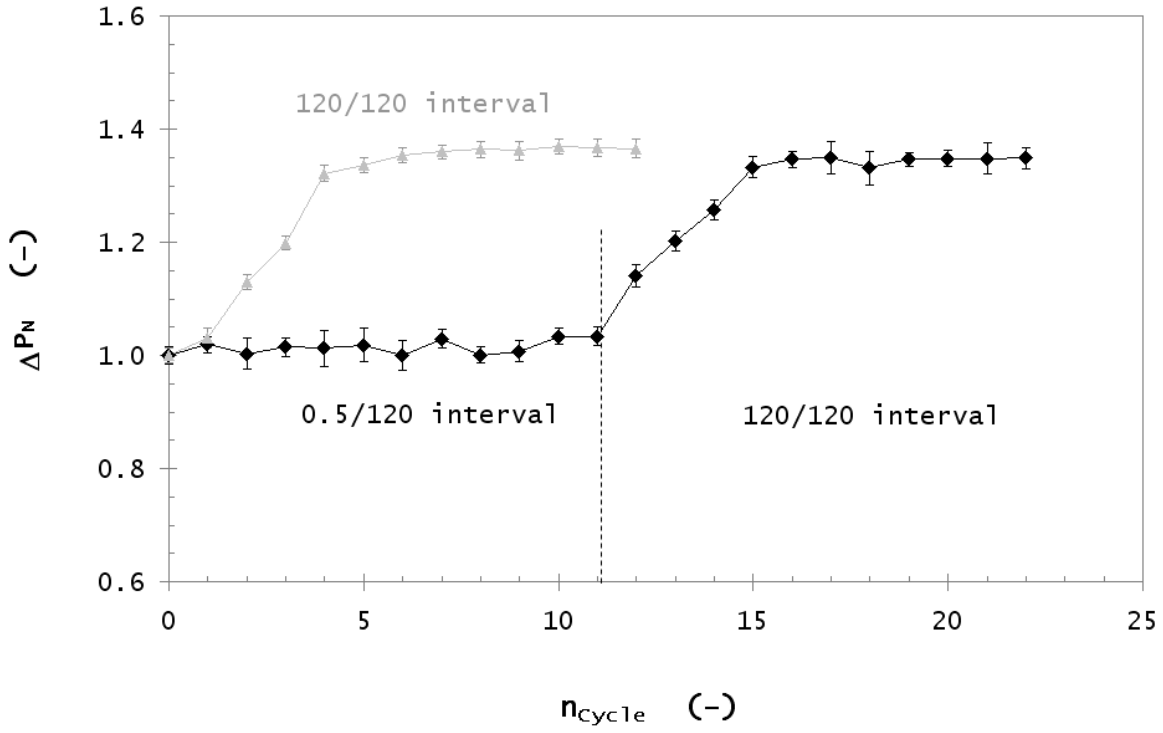

Fig. 6: Pressure drop behaviour of a filter (type A) during discontinuous operation. The stop-and-go interval was set to 0.5 minute break and 120 minutes air-flow (0.5/120 interval)

during the first 10 cycles before it was set back to the normal interval of 120/120. Also shown for comparison are the 120/120 experimental results.

The first stage of the experiment was conducted using a short break of 30 seconds between the “on” periods which were kept at 2 hours (0.5/120 interval) as per the previous experiments. After 10 cycles the experiment was then changed to the usual 2-hours stop-and-go interval (120/120 interval). The curves are averaged from three (for the black curve) and five (for the grey curve) repetitions and the error bars indicate that the variation between the repetitions was minimal.

The pressure drop during the first stage remained the same as the ΔP_{EQ1} level, until the interval was changed to 120 min breaks. Once the interval was set to 120/120, the pressure drop increased each cycle until ΔP_{EQ2} was reached, which lay approximately 35% higher than ΔP_{EQ1}. The Saturation S_{EQ2} at this point was 0.73 compared to S_{EQ1} of 0.61. Both values correspond well with the results observed during experiments with a 120/120 interval from the end of the steady-filtration period.

This experiment supports the concept that the observed increase of pressure drop and saturation is induced by a rearrangement of liquid in the filter during breaks in airflow. If the air flow is recommenced before the oil has been displaced significantly, then no measurable changes in pressure drop will occur.

The type A filters consisted of 4 layers of fibres of the same diameter. Experiments were also conducted with type B filters (which consisted of media containing 2 different fibre diameters). The type B results showed the same general relationship as the type A filters.

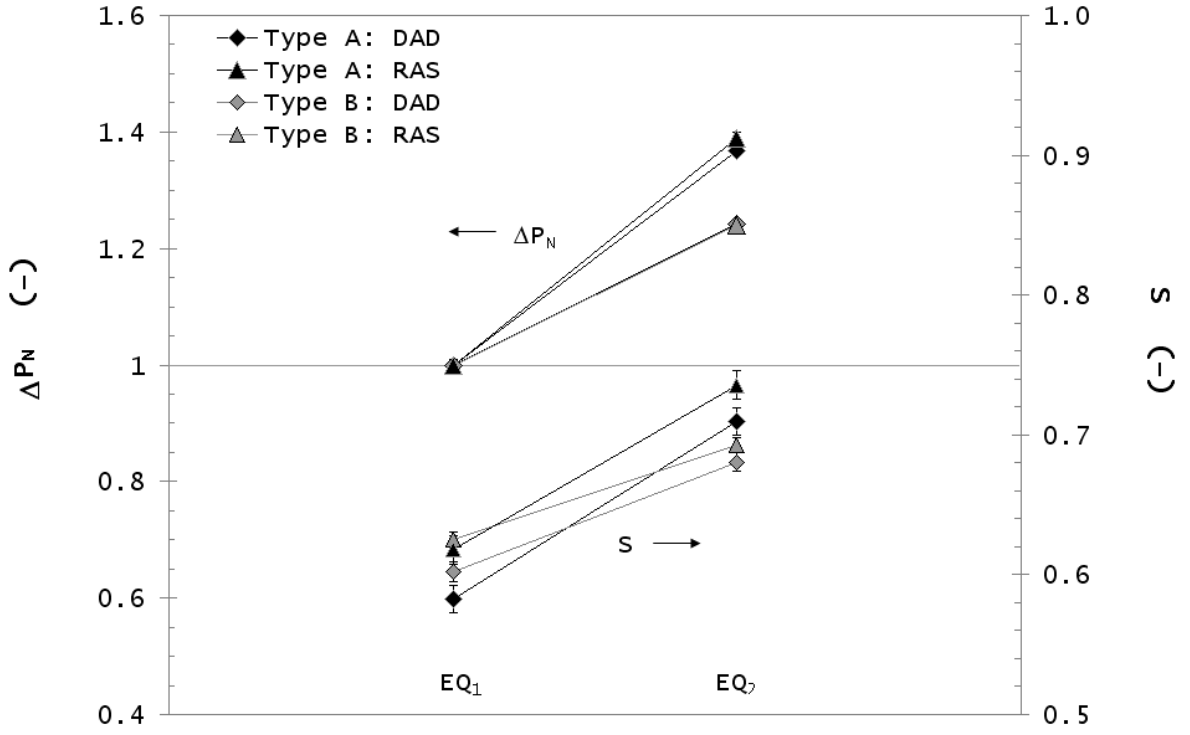

Fig. 7: Normalized pressure drop ΔP_N and saturation S at the first (EQ_1) and the second (EQ_2) equilibrium state for filters of type A and B. The filters were preloaded using the DAD or the RAS method.

The average values for the normalized pressure drop ΔP_N and the saturation *S* at the first (EQ_1) and the second (EQ_2) equilibrium state for filters of both types A and B are shown in Fig. 7. All filters were preloaded prior to discontinuous operation using either the *DAD* or the *RAS* method, data are based on approximately 20 experiments for each filter (40 filters total).

Again it can be observed that the preloading method did not influence the results, as the differences between both methods are generally within the range of the error bars. For filters of type A, an average increase of the pressure drop of 38% ±1% could be observed whereas filters of type B showed only 24% ±0.6%. Both filters showed a marginally higher saturation if the filter was preloaded using the *RAS* method. An increase in the saturation from 0.61 ±0.02 to 0.72 ±0.02 could be observed between the two equilibrium states for filters of type A and from 0.61 ±0.01 to 0.69 ±0.01 for filters of type B respectively.

As can be observed in Table 1 the type B filters possess a lower packing density (0.019) than the type A filters (0.023) - a difference of approximately 20%. This would mean that the type B filters would on average have larger interstices between the fibres, and a greater equivalent capillary diameter. This is the most likely explanation of approximately 40% difference in pressure drop and saturation increase between EQ_1 and EQ_2 in the filters.

3.3 Filter regeneration using high velocity air

To increase filtration efficiency and reduce saturation, it is obviously advantageous to be able to remove the additional oil entrained during the stop-start operation, thereby "regenerating" the filter. It has been demonstrated that a completely saturated (*DAD*) filter will reach EQ_1 when operated continuously from the outset. However the question remains whether filters could be "artificially" cleaned by increasing the interstitial velocity sufficiently. Therefore, the regeneration of filters was examined in this phase of the work.

In dust filtration applications [11] a surface filter can be cleaned or regenerated using a jet of compressed air to remove the “cake” of particles clogging the filter. Once the filter cake is (partially) removed, the permeability of the filter increases significantly which lowers the flow resistance and thus the pressure drop across the filter. In the case of mist filters, it was previously observed [10] that particle-free purge air flowing through an oil filter with a higher velocity than the filtration velocity can lower the pressure drop by driving oil out of the filter. It is a logical extension therefore, that a modified form of “pulse-jet“ cleaning could be applied to oil mist filters in order to clean the clogged passages thus returning the filter to its initial condition (or very near).

Table 2: Preloading configuration for two filters (type A) that were cleaned and reused.

	Filter 1	**Filter 2**
1st test	DAD	RAS
2nd test	RAS	DAD
3rd test	DAD	RAS

Therefore, two type A filters were compared using different combinations of preloading methods as shown in TABLE 2. The filters underwent a preloading and an aerosol saturation stage as per normal. Once the first equilibrium state EQ_1 was reached, they were subjected to discontinuous operation as described earlier until the second equilibrium state EQ_2 was reached. The filters were then cleaned by a flow of high velocity air (compressed air “pulse-jet“) before the next round of preloading commenced. The preloading method alternated between the *DAD* and the *RAS* method, with one filter starting with the *DAD* method and the other with the *RAS* method.

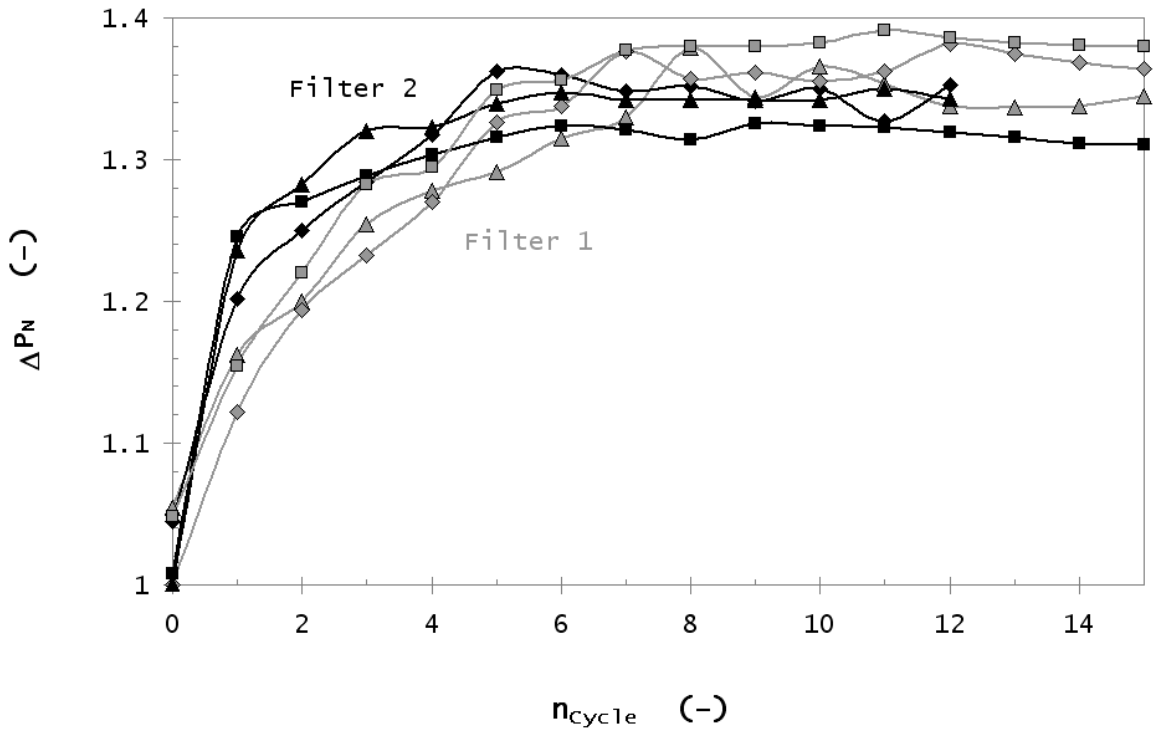

Fig. 8: Pressure drop behaviour of two filters with three repetitions of discontinuous operation. The filters were "pulse-jet" cleaned once they reached EQ_2 and subsequently preloaded with a different method before undergoing continuous and discontinuous operation again. Filter 1 (grey) was initially preloaded using the DAD method, the RAS method after the 1st regeneration and the DAD method again after the 2nd regeneration. Filter 2 (black) was initially preloaded using the RAS method followed by the DAD method after the 1st regeneration and the RAS method again after the 2nd regeneration. The three test stages are pictured by different markers (diamonds: first test, triangles: after 1st regeneration, squares: after 2nd regeneration)

The pressure drop of the first 15 filtration steps during discontinuous operation is shown in Fig. 8 for both filters. All pressure drop values are normalized to the first equilibrium state pressure drop ΔP_{EQ1} of the initial test and therefore the curves do not necessarily commence at 1 on the y axis for the second and third test. It can be seen that, regardless of the

preloading method, both filters show a similar behaviour for each test. As was also observed in earlier experiments the pressure increased during the first cycles and then reached a constant value ΔP_{EQ2} approximately 35% (±4%) greater than ΔP_{EQ1} for each curve. This value agrees well with the results of earlier experiments. The first equilibrium state pressure drop ΔP_{EQ1} of the following tests was 2-5% higher than the pressure drop for the initial tests, which corresponds to a pressure drop difference of less than 0.75 mbar.

Table 3: Filter saturation at the second equilibrium state S_{EQ2} and immediately after regeneration S_R (jet-velocity = 3 m/s) for different preloading methods

	DAD	**RAS**
S_{EQ2}	0.70 ±0.01	0.72 ±0.01
S_R	0.51 ±0.01	0.54 ±0.01

Due to the cleaning process using a compressed air jet, the filter saturation could be decreased from an average of 0.71 to 0.52 as can be seen in TABLE 3. The results were very similar for both preloading methods.

These findings led to further experiments to investigate the influence of different jet air pressures which in turn will induce different air flow velocities and therefore shear forces in the filter during cleaning. For the following experiments, filters of type A were saturated using the *DAD* preloading method and then continuously operated until the first equilibrium state was reached. The filters were then cleaned via a reverse “pulse-jet“ and once again operated continuously until they reached an equilibrium state (EQ_1) again. The process was repeated with a subsequently increased “pulse-jet“ pressure from 0.65 – 3.5 bar. The results of these experiments can be seen in Fig. 9. The pressure drop measurements were

conducted at the usual filtration rate of 55 LPM and all values represent the normalized pressure drop ΔP_N which is the ratio between the current pressure drop and the pressure drop present during the first equilibrium stage ΔP_{EQ1} (after the initial saturation). The experiment was repeated three times for each velocity and the results were averaged.

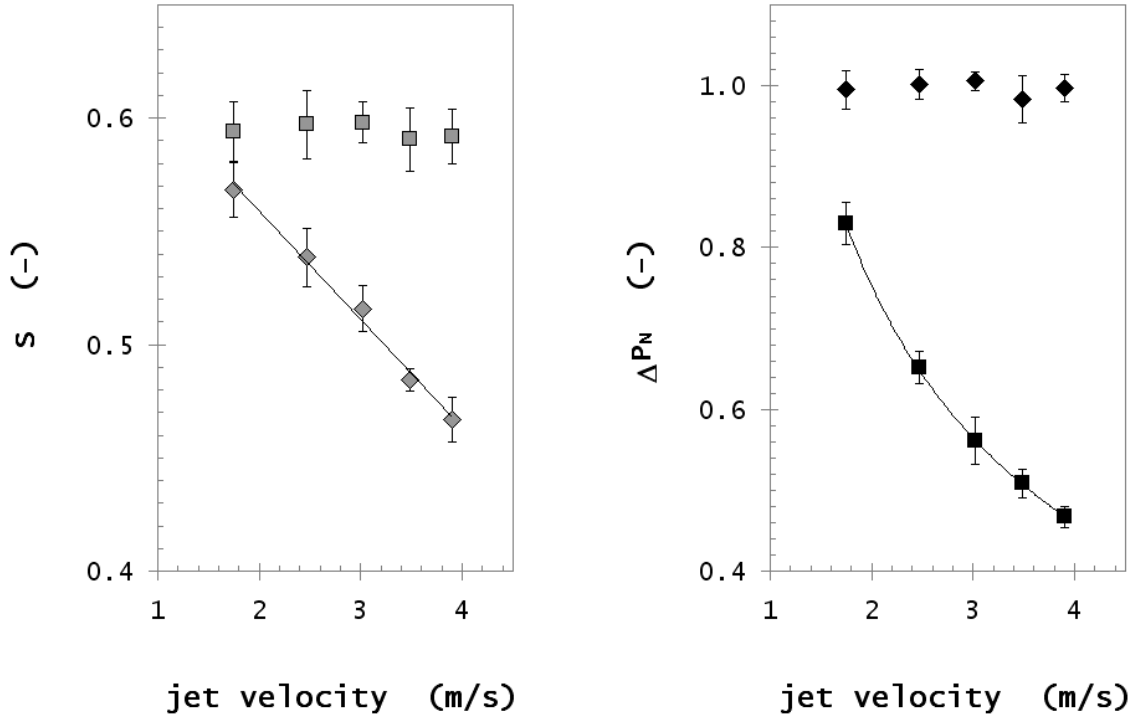

Fig. 9: Normalized pressure drop ΔP_N and saturation S immediately after the cleaning and after reaching EQ_1. The filters (type A) were cleaned using different velocities with a reverse "pulse-jet".

It can be seen that both saturation and pressure drop could be reduced after the filter was cleaned. The relationship between the saturation and the "pulse-jet" velocity appears to be linear in this experiment. However it is known from other works [12] that during filtration a "static" amount of oil remains in the filter that cannot be transported by shear forces. This means that the relationship shown above appears linear in the range between S = 0.45 to 0.6 but would likely follow a curve and eventually attain a constant, non-zero value – the

"static" saturation. The pressure drop after cleaning follows the "pulse-jet" velocity in a curve ($\Delta P_N = 1.24\, v^{-1/\sqrt{2}}$). Therefore the current results agree with the "static" saturation theory and suggests that ΔP_N will eventually plateau.

Furthermore, it could be shown that the filter was able to attain very similar equilibrium conditions ($\Delta P_{N,EQ1}$ and S_{EQ1}) after each cleaning process. This finding was also observed in earlier experiments as discussed in Fig. 8.

3.4 Phenomenological filter cleaning model

Earlier experiments showed that fully saturated (i.e. preloaded using the *DAD* method) filters lost significant amounts of oil during the initial seconds of filtration. The high pressure drop and high interstitial air velocity likely provided sufficient force to drive the oil to the rear of the filter where it was able to drain. In order to model the flow of fluid in fibrous filters, they can be approximated by a bundle of vertical or horizontal capillary tubes [13], [14].

An analytical solution for capillary displacement in circular, horizontal tubes was derived by Washburn [15] using the Hagen-Poiseuille equation for laminar flow, neglecting inertial effects.

$$\frac{32\mu}{d_{cap}^2}\dot{l}(t) = \frac{P_{l,0} - P_{l,m}}{l(t)} \tag{4}$$

with μ being the dynamic viscosity of the liquid, d_{cap} the capillary tube diameter, $l(t)$ the distance of the gas-liquid interface from the tube inlet (depending on the time t) and $\dot{l}(t)$ its derivation (i.e. dl(t)/dt). $P_{l,0}$ and $P_{l,m}$ the liquid pressure at the start of the capillary and at the gas-liquid interface respectively. For vertical capillary systems, an additional term is needed to include gravitational forces.

The capillary pressure, which is the pressure difference between the gas pressure P_g and the liquid pressure $P_{l,m}$ is given by the Young-Laplace equation as follows

$$P_g - P_{l,m} = \frac{4\gamma}{d_{cap}} \cos\theta \tag{5}$$

with γ being the interfacial tension between the gas and the liquid and θ the contact angle of the liquid-solid interface (which was determined as 79 ° in previous work [16]).

Combining these two equations leads to an ordinary differential equation for the distance of the meniscus from the start of the capillary and the resulting pressure drop ΔP

$$\Delta P = P_g - P_{l,0} = \frac{4\gamma}{d_{cap}} \cos\theta - \frac{32\mu}{d_{cap}^2} \dot{l}(t) l(t) \tag{6}$$

By assuming that the contact angle θ is constant over time (as assumed by Washburn) this equation can be solved and an expression for the distance of the meniscus from the capillary inlet dependant on pressure drop, time and capillary diameter can be obtained as follows

$$l(t) = \sqrt{\frac{\gamma \cos\theta}{4\mu} d_{cap} - \frac{\Delta P}{16\mu} d_{cap}^2}\sqrt{t} \tag{7}$$

Although this equation was developed for liquid penetration into a capillary it seems reasonable to use the same equation for the displacement of liquid in a capillary [17].

We assume that the horizontal capillary in this case is initially filled and is then acted on by a pressure differential. With equation (7), the ratio of the emptied length of a capillary of a certain diameter can be calculated if the pressure drop behaviour over time is known (as is the case in this work). Since the filter can be represented by a bundle of horizontal capillary tubes of known diameter distribution and length, it is possible to calculate the ratio of the emptied capillary space in the whole filter and thus the filter saturation as a function of the pressure drop during the capillary draining process

The assumptions that were made for modelling are as follows:

- All capillaries are of the same length (the filter thickness)
- The capillary diameter distribution is a normal distribution
- The filter is fully saturated at the commencement of filtration (i.e. all capillaries are fully filled)

The filter saturation for every time step (100ms) during cleaning of the fully saturated filter was calculated (S_{calc}) as the amount of remaining liquid in each capillary in relation to the capillary length weighted by the abundance of every capillary diameter as given by the

normal distribution. The amount of liquid in each capillary was calculated using equation (7) and by multiplying the distance of the meniscus from the capillary inlet by the cross sectional area of the capillary. Additionally, the experimental saturation (S_{exp}) was calculated based on the mass of liquid collected draining from the filter.

Previously published work [16] investigated capillary rise height using (stainless steel) fibrous filters of a type almost identical to those used in the current work. Thus it seems reasonable to utilise the empirical equations for the determination of the capillary diameter developed in the work mentioned above to the current filter media. If the fibre diameter and the packing density of the filter are known, the average capillary diameter during the initial (acceleration) regime can be estimated as

$$\frac{d_{cap}}{2} = -36.5 \ln\left(\frac{2\alpha}{\mathrm{d_f}}\right) - 122.5 \tag{8}$$

Using this diameter as the mean diameter d_{mean} = ~80 µm of the capillary distribution with a standard deviation of σ = 20 (from [16]) a normal distribution was obtained which was used as basis for model determination.

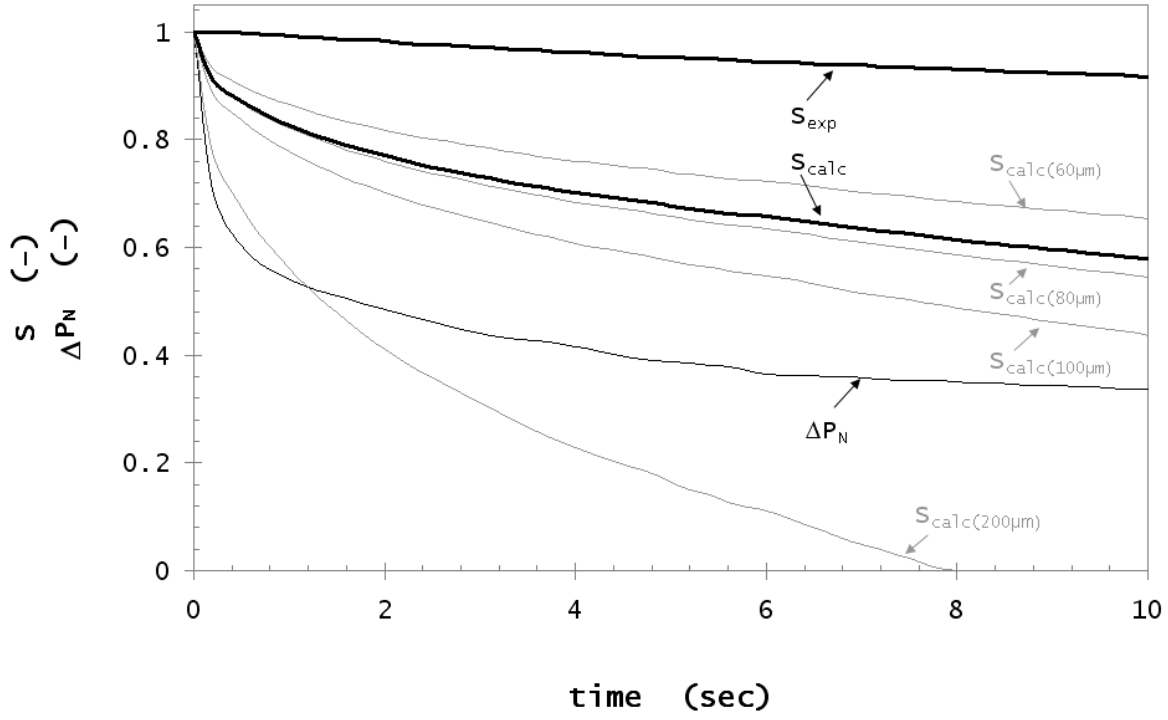

Fig. 10: Calculated (S_{calc}) and experimental saturation (S_{exp}) and normalized pressure drop (ΔP_N) during filter cleaning. The saturation for three specific capillary diameters d_{mean} (80µm), d_{mean}-σ (60µm), d_{mean}+σ (100µm) and a comparatively large capillary of 200 µm was modelled.

Fig. 10 shows the experimental (S_{exp}) and theoretical capillary model saturation (S_{calc}) values for the first 10 seconds of the filter cleaning / drainage for a fully saturated type A filter.

As can be seen, the pressure drop decreased to approximately 30% of the initial value during this time which corresponds to approximately 21 mbar. Although earlier experiments have shown that the pressure drop decreased further to approximately 15 mbar (as was described earlier in this work) during the remaining hour of the experiment, 90% of the total pressure drop decrease took place within the first 10 seconds thus this time frame was

selected as being sufficiently representative for the evaluation of the phenomenological model.

Fig. 10 also shows the normalised pressure drop (ΔP_N). The four additional S_{calc} curves show the theoretical drainage of the mean and ±1 standard deviation (from the mean) capillary diameter and for comparison a relatively large (200µm) capillary respectively. The experimental data shown is representative of the results found over multiple experiments. It can be seen that the saturation for all capillaries decreased most rapidly during the initial seconds when the air flow commenced. This corresponds well with findings published in other works [16], [19] which showed that an “acceleration phase” occurs during initial capillary rise or fall, which decreases over time to a slower rate. The capillary with the largest diameters shows the fastest decrease in saturation and is completely cleaned after approximately 8 seconds, whereas the smallest capillary has only been cleaned down to approximately 75% at the same time. This suggests that the liquid can move more easily in capillaries of a large diameter than in capillaries of small diameter which corresponds to the observations in other works where it was shown that the capillary rise height increased faster in larger capillaries [16], [20]. This finding also supports the findings discussed in Fig. 9. Larger capillaries are cleaned first causing a quick initial pressure drop decrease, whereas it takes increasingly more effort to clean capillaries of decreasing diameters.

The difference between the theoretical and experimental saturation curve can be explained by the fact that the actual drained oil is only measured by the balance once it has completely drained to the bottom of the filter and then dripped into the collection canister on the balance which is suspected to lead to a time lag in the mass measured. Furthermore, it is possible that in the experimental case, the ends of cleaned capillaries may be clogged by oil draining

from capillaries above (and flowing down the rear of the filter). This is assumed to affect the lower parts of the filter more, for obvious reasons.

It can be said that the phenomenological filter model is able to describe initial drainage during filter cleaning and show a relationship between saturation and pressure drop. However the model does not appear to capture all the processes occurring in the filter, so at this stage must be regarded as a descriptive, rather than predictive, model. It is likely that over the longer term, as S_{exp} decreases the magnitude of forces may change such that capillarity becomes less significant.

4 Conclusions

This work has investigated the influence of discontinuous aerosol flow during the filtration process of liquid aerosols using two different types of fibrous media. It has been found that both types of filters tested undergo a second loading stage beyond the first equilibrium state if they are not operated continuously and reach a second equilibrium point with an increase in pressure drop of 24% and 38% respectively and a saturation increase of 8% and 12% between the two equilibrium states. This was attributed to a rearrangement of liquid in the filter during the breaks, clogging previously free passages. This process was mainly driven by capillary forces. The ratio of shear and capillary forces was found to define whether these passages were able to be cleaned once aerosol flow was recommenced.

Based on these findings, the influence of different air flow velocities during the cleaning process of a fully saturated filter by a pulse of compressed air in the flow direction was investigated

It was found that filters could be cleaned to a certain (constant) level and be “reused" subsequently. It was also observed that they attained the same equilibrium state after further use, even if the filters were saturated using different preloading techniques.

A simple phenomenological model based on the Lucas-Washburn equation was developed to describe drainage of supersaturated filter media. It was shown that capillary theory appears to describe the process which occurs as liquid is drained from supersaturated filters, at least during the initial phases.

The experiments conducted in this work represent a more realistic test for oil-mist (or coalescing) filters than typical laboratory testing. Furthermore, it is hoped that this work will help to bridge the gap between laboratory and field test results.

Acknowledgement:

The authors would like to acknowledge financial support from the Australian Research Council (LP0883877) and MANN+HUMMEL GmbH.

Appendix A1: Derivation of Equation (7)

$$\Delta P = P_g - P_{l,0} = \frac{4\gamma}{d_{cap}}\cos\theta - \frac{32\mu}{d_{cap}^2}\dot{l}(t)l(t) \tag{6}$$

Rearranging:

$$\dot{l}(t) = \left(\frac{4\gamma}{d_{cap}}\cos\theta - \Delta P\right) \Big/ \left(\frac{32\mu}{d_{cap}^2}l(t)\right)$$

with $\dot{l}(t) = \frac{dl}{dt}$:

$$\frac{dl}{dt} = \left(\frac{4\gamma}{d_{cap}}\cos\theta - \Delta P\right) \Big/ \left(\frac{32\mu}{d_{cap}^2}l(t)\right)$$

Separation of variables:

$$l(t)dl = \left(\frac{4\gamma}{d_{cap}}\cos\theta - \Delta P\right) \Big/ \left(\frac{32\mu}{d_{cap}^2}\right) dt$$

Integration leads to:

$$\frac{1}{2}l^2(t) = \left(\frac{4\gamma}{d_{cap}}\cos\theta - \Delta P\right) \Big/ \left(\frac{32\mu}{d_{cap}^2}\right) t$$

Rearranging and extracting the root:

$$l(t) = \sqrt{2\left(\frac{4\gamma}{d_{cap}}\cos\theta - \Delta P\right) \Big/ \left(\frac{32\mu}{d_{cap}^2}\right) t}$$

Rearranging:

$$l(t) = \sqrt{\frac{\gamma \cos\theta}{4\mu} d_{cap} - \frac{\Delta P}{16\mu} d_{cap}^2}\sqrt{t} \quad (7)$$

References:

[1] P. Contal, J. Simao, D. Thomas, T. Frising, S. Callé, J.C. Appert-Collin, D. Bémer, Clogging of fibre filters by submicron droplets. Phenomena and influence of operating conditions, Journal of Aerosol Science, 35 (2004) 263-278.
[2] D.C. Walsh, J.I.T. Stenhouse, K.L. Scurrah, A. Graef, The effect of solid and liquid aerosol particle loading on fibrous filter material performance, Journal of Aerosol Science, 27 (1996) S617-S618.
[3] R.-J. Roe, Wetting of fine wires and fibers by a liquid film, Journal of Colloid and Interface Science, 50 (1975) 70-79.
[4] B.J. Mullins, G. Kasper, Comment on: "Clogging of fibrous filters by liquid aerosol particles: Experimental and phenomenological modelling study" by Frising et al, Chemical Engineering Science, 61 (2006) 6223-6227.
[5] P.C. Raynor, D. Leith, The Influence of Accumulated Liquid on Fibrous Filter Performance, Journal of Aerosol Science, 31 (2000) 19-34.
[6] T. Frising, D. Thomas, D. Bémer, P. Contal, Clogging of fibrous filters by liquid aerosol particles: Experimental and phenomenological modelling study, Chemical Engineering Science, 60 (2005) 2751-2762.
[7] J.R. Conder, T.P. Liew, Fine mist filtration by wet filters - II: Efficiency of fibrous filters, Journal of Aerosol Science, 20 (1989) 45-57.
[8] W.W.-F. Leung, C.-H. Hung, Investigation on pressure drop evolution of fibrous filter operating in aerodynamic slip regime under continuous loading of sub-micron aerosols, Separation and Purification Technology, 63 (2008) 691-700.
[9] S. Payet, D. Boulaud, G. Madelaine, A. Renoux, Penetration and pressure drop of a HEPA filter during loading with submicron liquid particles, Journal of Aerosol Science, 23 (1992) 723-735.
[10] T. Frising, D. Thomas, J.-C. Appert-Collin, S. Callé-Chazelet, P. Contal, Influence of Liquid Aerosol Stop-and-Go on the Performance of Fibrous Filters, FILTRATION, 5 (2005) 9.
[11] A. Dittler, G. Kasper, Simulation of operational behaviour of patchily regenerated, rigid gas cleaning filter media, Chemical Engineering and Processing, 38 (1999) 321-327.
[12] D. Kampa, A Model for Steady-State Oil Transport and Saturation in a Mist Filter, in: 18th World IMACS / MODSIM Congress, Cairns, Australia, 2009.
[13] M. Denesuk, G.L. Smith, B.J.J. Zelinski, N.J. Kreidl, D.R. Uhlmann, Capillary Penetration of Liquid Droplets into Porous Materials, Journal of Colloid and Interface Science, 158 (1993) 114-120.
[14] M. Hilpert, Effects of dynamic contact angle on liquid infiltration into inclined capillary tubes: (Semi)-analytical solutions, Journal of Colloid and Interface Science, 337 (2009) 138-144.
[15] E.W. Washburn, The Dynamics of Capillary Flow, Physical Review, 17 (1921) 273.
[16] B.J. Mullins, R.D. Braddock, G. Kasper, Capillarity in fibrous filter media: Relationship to filter properties, Chemical Engineering Science, 62 (2007) 6191-6198.
[17] M. Hilpert, Effects of dynamic contact angle on liquid withdrawal from capillary tubes: (Semi)-analytical solutions, Journal of Colloid and Interface Science, 347 (2010) 315-323.
[18] T.P. Liew, J.R. Conder, Fine mist filtration by wet filters - I. Liquid saturation and flow resistance of fibrous filters, Journal of Aerosol Science, 16 (1985) 497-509.
[19] S. Jaganathan, H.V. Tafreshi, B. Pourdeyhimi, A realistic modeling of fluid infiltration in thin fibrous sheets, JOURNAL OF APPLIED PHYSICS, 105 (2009) 8.
[20] A. Marmur, R.D. Cohen, Characterization of Porous Media by the Kinetics of Liquid Penetration: The Vertical Capillaries Model, Journal of Colloid and Interface Science, 189 (1997) 299-304.